Atom-resolved electronic spectra for Alq_3 from theory and experiment

A. Curioni[a] and W. Andreoni
IBM Research Division, Zurich Research Laboratory, CH-8803 Rüschlikon, Switzerland

R. Treusch and F. J. Himpsel
Department of Physics, University of Wisconsin–Madison, Madison, Wisconsin 53706-1390

E. Haskal and P. Seidler
Zurich Research Laboratory, IBM Research Division, CH-8803 Rüschlikon, Switzerland

C. Heske
Advanced Light Source, Lawrence Berkeley National Laboratory, Berkeley, California 94720

S. Kakar, T. van Buuren, and L. J. Terminello
Lawrence Livermore National Laboratory, Livermore, California 94551

(Received 1 December; accepted for publication 2 February 1998)

The electronic structure of Alq_3 is investigated using density functional theory-based calculations, photoemission and near-edge x-ray absorption fine structure. The distinct features of the observed spectra are understood in terms of contributions from the different atoms and molecular orbitals. Fingerprints of the molecular bonding and of the individual atoms are identified. These results are meant to be a reference for the monitoring of chemical processes that Alq_3 may undergo during fabrication or degradation of light-emitting devices, and for the understanding of the effects of ligand or metal substitution. © *1998 American Institute of Physics.*
[S0003-6951(98)01813-0]

Tris-(8-hydroxyquinolate)-aluminum (Alq_3) is the key electroluminescent material currently used in organic light-emitting devices (OLEDs) based on ''small molecules''[1]. Since the first report in 1987[2] of an OLED based on Alq_3, a great effort has been made to control and improve its efficiency and durability, as well as to modify and extend the spectral range of light emission[3,4]. Our understanding of the electroluminescence mechanism and of the material-specific characteristics of the device is still poor. Here we present a joint theoretical and experimental characterization of the electronic structure of Alq_3, both in the occupied and in the unoccupied portions of the spectrum. Calculated spectra are analyzed in such a way that all features are ascribed to individual atoms and/or groups of atoms. This offers the unique possibility to use them as fingerprints of site-specific chemical reactions taking place in the device[5], such as degradation processes at the electrode/organic interface.

The occupied electron states of Alq_3 were investigated with soft x-ray photoelectron spectroscopy (SXPS) measurements performed with synchrotron radiation at a photon energy of 240 eV using an ellipsoidal mirror analyzer at the undulator beam line 8 at the Advanced Light Source (ALS), Berkeley. The unoccupied states were probed with near-edge x-ray absorption fine structure (NEXAFS). Absorption was measured for the C, N, O 1*s* levels, via the total electron yield mode at the ALS and at the Stanford Synchrotron Radiation Laboratory (SSRL). The Alq_3 films prepared by sublimation in ultrahigh vacuum were thick enough to suppress substrate emission, but thin enough to prevent charging[6].

Calculations were based on density-functional theory using gradient-corrected exchange correlation functionals[7], atomic pseudopotentials[8], and plane waves up to 70 Ry. The results we discuss here refer to the meridianal isomer in the optimized geometry (Fig. 1)[9]. This is the isomer observed in the crystal structures done so far[10], and the one that is slightly lower in energy ($\sim$4 kcal/mol). The properties we discuss here are only marginally dependent on the specific conformation of the molecule[9].

The spectral function of interest is the density of the one-electron states (DOS), which can be directly compared with valence-band photoemission. Although Kohn–Sham (KS) levels do not correspond to quasi-particle excitation energies, the DOS generally reproduces the photoemission spectra of molecular solids and semiconductors reasonably well and, in particular, their salient features in the range of a

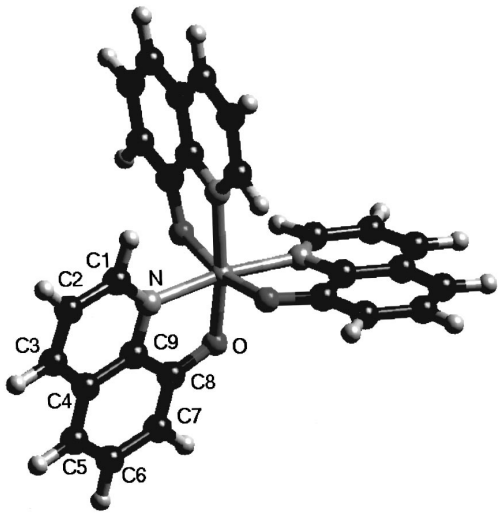

FIG. 1. Alq_3 structure of meridianal isomer.

[a]Electronic mail: cur@zurich.ibm.com

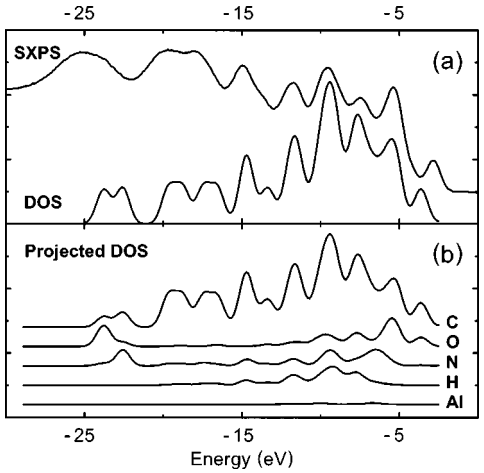

FIG. 2. (a) SXPS spectrum of Alq_3 and calculated valence DOS. (b) Projected valence DOS on the individual atomic species as labeled.

few eV below and above the Fermi level (E_F). Moreover, a description of the electronic structure in terms of the KS orbitals bears the correct character and localization properties. By projecting the KS states onto the atomic wave functions, we decompose the DOS into the contributions of all different elements [projected density of states, (PDOS)]. Our calculations are for the isolated Alq_3 molecule. For sake of comparison with the experiment, the discrete levels were broadened, using a Gaussian function with $\sigma = 0.5$ eV. The (P)DOS was also shifted so that the energy of the leading maximum matches that observed in the experiment.

The DOS and PDOS below and above E_F are illustrated in Figs. 2 and 3, respectively. The former compares well with the photoemission peaks: both shape and sequence are reproduced for at least 10 eV below the highest occupied molecular orbital (HOMO). Because Al is stripped of its valence electrons, its contribution to the DOS is negligible. The weak orbital density in Fig. 2(b) around Al corresponds to states on the ligands that are strongly polarized towards the central ion. The highly ionic character of the ligands–Al interaction accounts also for the instability of Alq_3 towards hydrolysis[11]. The peak at the highest binding energy in the photoemission spectrum (-28 to -22 eV) arises from the 2 *s* component of the σ bonding between O and N and the neighboring C's. The PDOS distinguishes between O and N components that merge into a single peak in the observed spectrum. The region between -21 and -7 eV corresponds to the remaining σ backbone. In fact it is dominated by carbons, and has contributions from hydrogen. More specifically, this region is divided into C 2*s* (-21 to -11 eV) and C 2*p* (-11 to -7 eV) components. The π states start to contribute at -9.5 eV. The N and O sp^2- and sp^3-derived lone pairs pointing towards Al are at -7 eV (right-hand shoulder of the peak at -7.3 eV) and at -5.4 eV, respectively. Therefore, both features can be considered fingerprints of the metal–ligands interactions.

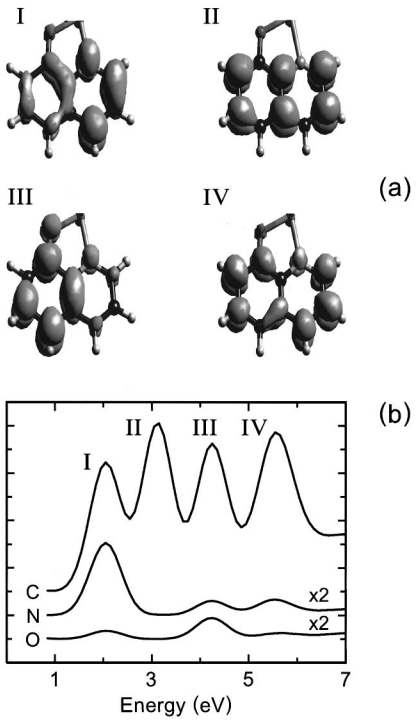

FIG. 3. (a) Probability isodensity surface (0.001 a.u.) of the LUMO (I), LUMO+1 (II), LUMO+2 (III) and LUMO+3 (IV) sets of orbitals. Only one ligand is shown. (b) Projected DOS calculated for these empty states.

Both the occupied and unoccupied π states of Alq_3 near the HOMO–LUMO gap group into sets (''triplets'') that have the same orbital character on each of the three ligands. A crucial feature is that the HOMO set is localized mainly on the phenoxide side of the ligands, whereas the lowest unoccupied molecular orbital (LUMO) set (I) [Fig. 3(a)] on the pyridyl side. This is reflected in the PDOS [Figs. 2(b) and 3(b)]: only a weak contribution comes from N to the photoemission peak at the lowest binding energy, and from O to the lowest peak in the spectrum of the unoccupied states. This implies that oxidizing agents will attack the molecule at the phenoxide side of the ligands, reducing agents at the pyridyl side. The LUMO+1 (II) and LUMO+3 (IV) sets are more uniformly distributed on the two sides [Fig. 3(a)]. Interestingly, the LUMO+1 set (II) vanishes on both N and O, whereas the LUMO+2 (III), although more localized on the phenoxide side, has a similar amplitude on both of them, Fig. 3(a). The contribution of Al to these unoccupied states is vanishingly small. Thus no direct role of the metal atom can be claimed in light-emission processes of Alq_3.

For the empty states the ideal experiment with which to compare the DOS would be inverse photoemission. Unfortunately, because of the low photoemission probability and hence the high electron bombardment required, Alq_3 undergoes decomposition under experimental conditions. However, an atom-resolved spectroscopy for the unoccupied states is NEXAFS, as shown in Fig. 4 for C, N, and O. By exciting electrons from a specific atomic core, NEXAFS probes dipole-allowed transitions to the virtual states and the localization of the latter. The position of the levels relative to E_F can be estimated by subtracting the binding energy of the core state from the photon energy.

A rather detailed interpretation of the core photoabsorption function is provided by

$$\alpha_c(E) \sim \sum_k \sum_i |\langle \phi_c^k \ |\mathbf{r}| \ \psi_i \rangle|^2 \ \frac{\delta(E_i - E_c^k - E)}{E}. \qquad (1)$$

c refers to 1*s* core states and the sum runs over all the atoms, *k*, of a given species and over the empty KS molecular or-

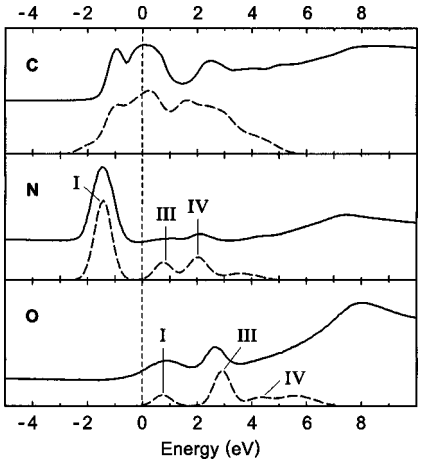

FIG. 4. 1*s* NEXAFS spectrum (solid) compared to calculated (dashed) photoabsorption, [Eq. (1)], for C, N, and O. The labels I–IV are as in Fig. 3.

bitals, i. Core atomic wave functions ϕ_c^k were derived from an all-electron calculation[12] of the optimized structure[9].

Equation (1) neglects several many-body effects, e.g. electronic relaxation and electron-hole interaction. Comparison with experiment can be made easier by simply aligning the first experimental and calculated peaks. The relative shifts of the C, N, and O first peaks result mainly from a different strength of the electron–hole attraction[13]. The largest shift pertains to N, where the amplitude of the LUMO is higher. Examination of the individual orbitals and analysis of the transitions in terms of couplings of all the different atoms in the molecule provide a complete explanation of the excitation spectrum over a range of ~5 eV (see Fig. 4). This involves transitions to the π^* states of the LUMO (I), LUMO+1 (II), LUMO+2 (III), and LUMO+3 (IV) ''triplets.'' We do not consider higher energies because our scheme becomes less accurate. Moreover, this portion of the excitation spectrum does not appear to be atom specific and thus is of limited interest to the purpose of this work.

In the case of carbon, the 1*s* levels of the chemically distinct atoms are spread over $\approx$1.9 eV (about a center of gravity $\tilde{\epsilon}_{\mathrm{C}1s}$) and correlate with the Mulliken atomic charges q_k. If we consider $E_c = \tilde{\epsilon}_{\mathrm{C}\,1s}$ in Eq. (1) for all C's, $\alpha_C(E)$ consists of four well-resolved peaks, fully analogous with the C-projected DOS in Fig. 3(b). However, the experimental situation, illustrated in Fig. 4, is more complex. Owing to the splitting of the core levels, the photoabsorption peaks involve the mixing of diverse transitions. Nevertheless, the main components can be assigned. The first peak observed is dominated by transitions to the LUMO of the C3 atoms in the pyridyl rings (see Fig. 1) ($\epsilon_{\mathrm{C}\,1s} \approx \tilde{\epsilon}_{\mathrm{C}\,1s}$; $q=-0.03$). The second is a mixture of transitions to the LUMO (I), LUMO+1 (II), and LUMO+2 (III) sets, with the maximum relative intensity pertaining to the C $1s\rightarrow$ LUMO+2 (III) of the C5 atoms of the phenoxide rings (Fig. 1) ($\epsilon_{\mathrm{C}\,1s} \approx \epsilon_{\mathrm{C}\,1s} + 0.8$ eV; $q=-0.07$). The third is mainly due to transitions to the LUMO+2 (III), especially from the C8 atoms (Fig. 1) ($\epsilon_{\mathrm{C}\,1s} \approx \tilde{\epsilon}_{\mathrm{C}\,1s} - 0.8$ eV; $q=0.2$).

In contrast, excitations from both N and O correspond to narrower peaks, because the three N's and three O's are almost equivalent chemically, and the spread of the 1*s* energies is one order of magnitude smaller than that of C. Thus, different one-electron transitions do not overlap, facilitating the interpretation of NEXAFS. In the case of nitrogen, the first intense peak is due to N $1s\rightarrow$ LUMO transitions, the less intense second and third features to the N $1s\rightarrow$ LUMO+2 (III) and N $1s\rightarrow$ LUMO+3 (IV), respectively, whereas the N $1s\rightarrow$ LUMO+1 (II) transition is missing. This result agrees with the considerations above, namely that the LUMO ''triplet'' (I) is mainly on the pyridyl side of the rings and polarized towards N, whereas the LUMO+1 (II) states have components only on the C's. The relative intensities simply correspond to the relative participation of N in the specific orbitals. In the case of oxygen, the two peaks observed correspond to transitions to the LUMO (I) and LUMO+2 (III), respectively. The transition to the LUMO+1 (II) is missing, as for N, and transitions to higher-energy π^* states are hidden in the σ spectral region. The relative intensities can simply be explained in terms of the relative amplitudes of the LUMO (I) and LUMO+2 (III) on O.

In conclusion, photoemission and NEXAFS data combined with theoretical atom-resolved spectra and a detailed description of the electronic states have provided a complete picture of the orbital structure of Alq_3. This opens the way to a precise monitoring of the organic through similar measurements. In fact, on the basis of the spectra presented here, one can now characterize site-specific reactions or interactions that Alq_3 may undergo in a device, identify specific effects of chemical substitutions, and ultimately help control and enhance device performance.

The authors are grateful to H. W. Lee, K. Pakbaz, and G. Fox for providing an Alq_3 sample. The experimental work was supported by the Director, Office of Energy Research, Office of Basic Energy Sciences, at LLNL under Contract No. W-7405-ENG-48 and by the NSF under Award Nos. DMR-9632527 and DMR-9531009.

[1] J. R. Sheats, H. Antoniadis, M. Hueschen, W. Leonard, J. Miller, R. Moon, D. Roitman, and A. Stocking, Science **273**, 884 (1996).
[2] C. W. Tang and S. A. Van Slyke, Appl. Phys. Lett. **51**, 913 (1987).
[3] P. E. Burrows, Z. Shen, V. Bulovic, D. M. McCarty, S. R. Forrest, J. A. Cronin, and M. E. Thompson, J. Appl. Phys. **79**, 7991 (1996).
[4] Y. Hamada, IEEE Trans. Electron Devices **44**, 1208 (1997).
[5] D. G. J. Sutherland, J. A. Carlisle, P. Elliker, G. Fox, T. W. Hagler, I. Jimenez, H. W. Lee, K. Pakbaz, L. J. Terminello, S. C. Williams, F. J. Himpsel, D. K. Shuh, W. M. Tong, J. J. Jia, T. A. Callcott, and D. L. Ederer, Appl. Phys. Lett. **68**, 2046 (1996).
[6] More experimental details will be given elsewhere, see R. Treusch, S. Kakar, C. Heske, T. van Buuren, L. J. Terminello, F. J. Himpsel, V. V. Dinh, H. W. Lee, K. Pakbaz, G. Fox and I. Jimenez, (unpublished).
[7] A. D. Becke, Phys. Rev. A **38**, 3098 (1988); C. Lee, W. Yang, and R. G. Parr, Phys. Rev. B **37**, 785 (1988).
[8] J. L. Martins and N. Troullier, Phys. Rev. B **46**, 1766 (1992).
[9] A. Curioni, M. Boero, and W. Andreoni (unpublished).
[10] I. Fujii, N. Hirayama, J. Ohtani, and K. Kodama, Anal. Sci. **12**, 153 (1996); H. Schmidbaur, J. Lettenbauer, D. L. Wilkinson, G. Muller, and O. Kumberger, Z. Naturforsch. B **46**, 901 (1991).
[11] F. Papadimitrakopoulos, X.-M. Zhang, D. L. Thomsen III, and K. A. Higginson, Chem. Mater. **8**, 1363 (1996).
[12] Gaussian 94, Rev. D. 4 (Gaussian, Inc., Pittsburgh, PA, 1995).
[13] J. A. Horsley, J. Stohr, A. P. Hitchcock, D. C. Newbury, A. L. Johnson, and F. Sette, J. Chem. Phys. **82**, 6099 (1985).